Bidentate Dicarboxylate Capping Groups and Photosensitizers Control the Size of IrO_2 Nanoparticle Catalysts for Water Oxidation†

Paul G. Hoertz, Yeong-Il Kim, W. Justin Youngblood, and Thomas E. Mallouk*

Department of Chemistry, The Pennsylvania State University, University Park, Pennsylvania 16802

Received: January 28, 2007; In Final Form: April 1, 2007

Dicarboxylic acid ligands (malonate, succinate, and butylmalonate) stabilize 2 nm diameter IrO_2 particles synthesized by hydrolysis of aqueous $IrCl_6^{2-}$ solutions. Analogous monodentate (acetate) and tridentate (citrate) carboxylate ligands, as well as phosphonate and diphosphonate ligands, are less effective as stabilizers and lead to different degrees of nanoparticle aggregation, as evidenced by transmission electron microscopy. Succinate-stabilized 2 nm IrO_2 particles are good catalysts for water photo-oxidation in persulfate/sensitizer solutions. Ruthenium tris(2,2′-bipyridyl) sensitizers containing malonate and succinate groups in the 4,4′-positions are also good stabilizers of 2 nm diameter IrO_2 colloids. The excited-state emission of these bound succinate-terminated sensitizer molecules is efficiently quenched on a time scale of ∼30 ns, most likely by electron transfer to Ir(IV). In 1 M persulfate solutions in pH 5.8 $Na_2SiF_6/NaHCO_3$ buffer solutions, the excited-state of the bound sensitizer is quenched oxidatively on the time scale of ∼9 ns. Electron transfer from Ir(IV) to Ru(III) occurs with a first-order rate constant of $8 \times 10^2\ s^{-1}$, and oxygen is evolved. The turnover number for oxygen evolution under these conditions was ∼150. The sensitizer−IrO_2 diad is thus a functional catalyst for photo-oxidation of water, and may be a useful building block for overall visible light water splitting systems.

Introduction

Visible light water splitting has been described as one of the "holy grails" of chemistry.[1] Efficient photocatalysts for water splitting could have real practical value for solar energy conversion. In addition, the lessons learned from the design and study of such photocatalysts would be relevant to other energy related problems, including fuel cell catalysis and the photochemical synthesis of fuels from feedstocks such as carbon dioxide.

Recently, much progress has been made in the synthesis of visible-light absorbing oxide semiconductor particles that are stable under the conditions of water photolysis. By doping wide band gap oxides with nitrogen[2−4] or by making intergrowth structures with oxides of post-transition elements such as Bi,[5] the band gap can be shifted into the visible part of the spectrum. Heterogeneous oxide particles that contain p−n junctions[6] or metal−semiconductor junctions[7] have been shown to be active for light driven hydrogen or oxygen evolution and, in some cases, for overall water splitting.[8−12] Unfortunately, the efficiency of these photocatalysts, especially for water splitting, is generally low. It is also challenging to improve on the design of composite nanoparticles by correlating structural details, which are often difficult to image and control at the molecular level, with the dynamics of charge separation, recombination, and catalysis.

An alternative approach to using completely solid-state photocatalysts is to design hybrid systems, in which molecules perform some of the functions of light absorption, charge separation, and catalysis. Relying on the extensive body of knowledge developed in the study of dye-sensitized photoelectrochemical cells, one can design dye molecules that absorb visible light and efficiently separate charge at the molecule/oxide interface. Using this approach, we demonstrated that one could generate hydrogen photochemically from nonsacrificial electron donors when the sensitized oxide was coupled to nanoparticle catalysts for the H_2/H^+ interconversion. Coupling molecular sensitizers to oxygen-evolving catalysts for overall water splitting has however been a persistently difficult problem.[13−15] The known molecular catalysts for oxygen evolution require high overpotentials or turn over too slowly to compete with back electron-transfer reactions in microheterogeneous systems.[16−18] Inorganic catalysts, especially IrO_2, have faster turnover rates and generate oxygen at lower overpotential. Recently, we have shown that 10−30 nm diameter IrO_2 nanoparticles have turnover rates that are only 1−2 orders of magnitude slower, per surface atom, than the manganese oxo clusters in Photosystem II.[19,20] Although IrO_2 nanoparticles are interesting catalysts for overall water splitting, it is unfortunately not straightforward to couple them directly to sensitizer molecules at the oxide photocatalyst surface.

In this paper, we describe a new strategy for controlling the size of IrO_2 nanoparticles using bidentate dicarboxylate (malonate or succinate) capping groups. With these ligands, it is possible to stabilize 2 nm diameter particles, which are good catalysts for oxygen evolution from aqueous solutions of oxidized $[Ru(bpy)_3]^{2+}$ (bpy = 2,2′-bipyridine) and related photosensitizers. By using sensitizer molecules that contain pendant succinate or malonate groups, one can tether the sensitizer directly to the IrO_2 nanoparticle surface. In this case, there is strong electronic coupling and the excited-state of the sensitizer molecule is efficiently quenched by electron transfer to IrO_2. However, this process can be intercepted in solutions that contain persulfate, which oxidatively quenches the IrO_2-bound sensitizer molecule. In this case, efficient oxygen evolution results. The sensitizer-stabilized IrO_2 catalyst particles

† Part of the special issue "Norman Sutin Festschrift".

* To whom correspondence should be addressed.

10.1021/jp070735r CCC: $37.00
Published on Web 06/14/2007

are therefore interesting building blocks for overall water photolysis systems based on sensitized oxide semiconductor particles.

Experimental Section

Materials. Potassium hexachloroiridate, $RuCl_3 \cdot xH_2O$, sodium hydrogen citrate, malonic acid, succinic acid, glutaric acid, diethylaminomalonate hydrochloride, aspartic acid dimethyl ester hydrochloride, phthalic acid, butylmalonic acid, sodium acetate, aspartic acid, tetramethyl-1,2-phenylenediphosphonate, 1-hydroxyethylidinediphosphonic acid, thionyl chloride, anhydrous hexanes, dimethylformamide, HPF_6, ammonium hexafluorophosphate, tributylamine, THF, LiCl, sodium sulfate, sodium persulfate, sodium hexafluorosilicate, ascorbic acid, and diethyl ether were purchased and used as received. Dialysis was performed using molecular weight cutoff (MWCO) = 1000 Dalton cellulose membranes (Spectra/Por 7 Membranes; delivered wet in 0.1% sodium azide; available from VWR). The following compounds were prepared according to previous literature reports: 4,4′-dicarboxylic acid-2,2′-bipyridine ($dcbH_2$),[21] 4,4′-dicarbonyl chloride-2,2′-bipyridine,[22] 4,4′-diphosphonic acid-2,2′-bipyridine (dpbpy),[23] $Ru(bpy)_2Cl_2 \cdot 2H_2O$,[24] $Ru(dcbH_2)_2Cl_2$,[25] $Ru(dpbpy)_2Cl_2$,[26] $[Ru(bpy)_2(dcbH_2)](PF_6)_2$,[27] and $[Ru(dcbH_2)_2(bpy)](PF_6)_2$.[28] $[Ru(bpy)_3](PF_6)_2$ was prepared by metathesis of $[Ru(bpy)_3](Cl)_2$ (Aldrich) using ammonium hexafluorophosphate in H_2O. UV−vis spectra for ligands were conducted in EtOH while those for Ru compounds were performed under aqueous conditions. UV−vis data for a selection of Ru compounds is listed in Table S1.

Synthesis. 1,2-Phenylenediphosphonic Acid Disodium Salt. Tetramethyl-1,2-phenylenediphosphonate (3.2 g, 11 mmol) was added to conc. HCl (aq) (50 mL) and heated at reflux for 18 h. The solution was neutralized with sodium hydroxide and then treated with enough isopropanol to completely precipitate NaCl (s). The solution was then rotoevaporated to dryness. ^{1}H NMR δ (D_2O): 7.80−7.91 (m, 2H), 7.50−7.56 (m, 2H).

4,4′-(CONH-MA(OEt)$_2$)$_2$-2,2′-bipyridine [bpy(CONHMA(OEt)$_2$)$_2$]. Diethylaminomalonate hydrochloride (3.0 g, 14 mmol) was added to anhydrous THF (10 mL) followed by tributylamine (4.2 g, 23 mmol) in a 125 mL Erlenmeyer flask. 4,4′-dicarbonyl chloride-2,2′-bipyridine (1 g, 4 mmol) was slowly added over a period of 20 min while the reaction solution was sonicated (kept below 35 °C with ice), each time removing a rubber septum to keep out moisture. A white solid formed during the addition and was isolated by vacuum filtration and rinsed with THF followed by diethyl ether (1.5 g, 70%). ^{1}H NMR δ (d_6-DMSO): 9.75 (d, 2H), 8.78 (d, 2H), 8.70 (s, 2H), 7.75 (dd, 2H), 5.20 (d, 2H), 4.10 (m, 8H), 1.10 (t, 12H). λ_{abs} (nm): 238, 294.

4,4′-(CONH-SA(OMe)$_2$)$_2$-2,2′-bipyridine [bpy(CONHSA(OMe)$_2$)$_2$]. This compound was prepared in the same manner as bpy(CONHMA(OEt)$_2$)$_2$ using 4,4′-dicarbonyl chloride-2,2′-bipyridine (1.5 g, 5.3 mmol), aspartic acid dimethyl ester hydrochloride (4.22 g, 21.4 mmol), tributylamine (6.33 g, 34.2 mmol), and THF (10 mL) (1.48 g, 49%). ^{1}H NMR δ ($CDCl_3$): 8.83−8.90 (m, 4H), 7.82−7.85 (m, 2H), 7.60−7.66 (m, 2H), 5.11−5.19 (m, 2H), 3.86 (s, 6H), 3.77 (s, 6H), 3.03−3.26 (m, 4H). λ_{abs} (nm): 240, 294.

[bpy(CONHMA)$_2$](Na)$_4$. Bpy(CONHMA(OEt)$_2$)$_2$ (0.22 g, 0.39 mmol) was added to 0.5 M NaOH (aq) and stirred for 12 h at room temperature. The pH was adjusted to 7 with $HClO_4$ (aq). Acetone was then added to precipitate the tetra-anionic product. ^{1}H NMR δ (D_2O): 8.77 (d, 2H), 8.45 (s, 2H), 7.85 (dd, 2H). The resonance corresponding to the malonic position was not observed, presumably due to H/D exchange with the solvent.

[Ru(dcbH$_2$)$_3$](Cl)$_2$. $RuCl_3 \cdot xH_2O$ (0.5 g) and $dcbH_2$ (1.42 g, 5.8 mmol) were refluxed in DMF (12.5 mL) under N_2 for 18 h. Ascorbic acid (0.5 g) was added to the room-temperature reaction solution which was then refluxed for an additional 4 h. A brick-red solid was isolated by vacuum filtration. The solid was recrystallized several times by neutralizing an aqueous suspension with NaOH (aq) and then adding HCl (aq) to reprecipitate at pH = 2−3. ^{1}H NMR δ (D_2O/NaOD): 8.70 (3H, d), 8.57 (3H, dd), 8.19 (3H, m), 7.70 (3H, d), 7.66 (3H, dd), 7.50 (3H, dd).

[Ru(bpy)$_2$(bpy(CONHMA)$_2$)](Na)$_2$. $[Ru(bpy)_2Cl_2] \cdot 2H_2O$ (0.3 g, 0.6 mmol) and bpy(CONHMA(OEt)$_2$)$_2$ (1.1 equiv) were refluxed in 4:1 EtOH/H_2O (10 mL) under N_2 for 48 h. Upon cooling to room temperature, H_2O (50 mL) was added to precipitate excess ligand which was subsequently removed by filtration. Excess NH_4PF_6 (aq) was then added to the filtrate forming a red precipitate that was isolated by vacuum filtration and rinsed with deionized H_2O followed by diethyl ether. The precipitate was dissolved in 0.1 M NaOH (aq) and stirred for 12 h at room temperature. $HClO_4$ (aq) was then added until the pH reached 7; isopropanol was added to precipitate the product. ^{1}H NMR δ (D_2O): 8.85−9.02 (m, 2H), 8.42−8.49 (m, 4H), 7.91−8.02 (m, 6H), 7.62−7.75 (m, 6H), 7.24−7.33 (m, 4H). The resonance corresponding to the malonic position was not observed, presumably due to H/D exchange with the solvent.

[Ru(bpy)$_2$(bpy(CONHSA)$_2$)](Na)$_2$. This compound was prepared following the procedure for $[Ru(bpy)_2(bpy(CONHMA)_2)](Na)_2$. ^{1}H NMR δ (D_2O): 8.84−8.95 (m, 2H), 8.42−8.49 (m, 4H), 7.88−8.02 (m, 6H), 7.67−7.74 (m, 4H), 7.57−7.63 (m, 2H), 7.25−7.33 (m, 4H), 4.57 (dd, 2H), 2.53−2.81 (m, 4H).

Ru(LL)$_2$(bpy(CONH-DCA)$_2$) (DCA = MA, SA; LL = dcbH$_2$, dpbpy). These compounds were prepared following the procedure for $[Ru(bpy)_2(bpy(CONHMA)_2)](Na)_2$, using the corresponding $Ru(LL)_2Cl_2$ precursors and bpy(CONH-DCA-(OR)$_2$)$_2$ ligands. For final neutralization, $HClO_4$ (aq) was added to achieve pH 1.5 (for LL = dpbpy) or pH 7 (for LL = $dcbH_2$). Isopropanol was then added to precipitate the products, which were filtered and rinsed with isopropanol. The solids were dried under vacuum at 80 °C. $Ru(dpbpy)_2(bpy(CONHMA)_2) \cdot 2H_2O \cdot 2(iPrOH)$: Elem. Anal. Calcd: C, 39.09; H 4.03; N, 8.29. Found: C, 39.20; H 4.42; N, 8.28. $Ru(dpbpy)_2(bpy(CONHSA)_2) \cdot 5H_2O \cdot 2(iPrOH)$: Elem. Anal. Calcd: C, 39.02; H 4.41; N, 7.91. Found: C, 38.71; H 4.28; N, 7.66. $[Ru(dcb)_2(bpy(CONHSA)_2)](Na)_6 \cdot 8H_2O$: Elem. Anal. Calcd: C, 39.50; H 3.16; N, 8.38. Found: C, 39.69; H 3.72; N, 7.95.

Organic Surfactant−IrO_2 Nanoparticle Synthesis. In a typical synthesis, K_2IrCl_6 was added to an aqueous solution containing a particular organic surfactant followed by brief sonication; the Ir concentration was 1.24 mM. The surfactant:Ir molar ratio was varied to study its influence on particle growth. The pH of the solution was then adjusted with NaOH (aq) to achieve pH 10. The solution was heated in an Erlenmeyer flask at the desired temperature (typically 90 °C) for a certain amount of time (typically 10−20 min). The progress of particle formation was monitored ex situ by UV−visible spectroscopy by removing small 5 mL aliquots and quickly cooling them in an ice−H_2O bath. After heating for 10−20 min, the solution was cooled to room temperature with a cold water bath and then dialyzed against 2 L deionized water using a cellulose membrane. For ≥10 nm

particles, dialysis was carried out with MWCO = 12−14 kD membranes; for <10 nm particles, MWCO = 1 kD membranes were used.

Sensitized IrO_2 Nanoparticle Synthesis. The procedure was identical to the one used for making organic surfactant−IrO_2 nanoparticles with one exception. Dialysis was first performed against 2 L of 0.1 M Na_2SO_4 (aq) in order to screen the negatively charged cellulose membranes allowing for passage of highly anionic, unbound Ru sensitizers. Dialysis was continued until the external dialysis solution remained colorless. At this point, the UV−vis absorbance spectrum of the sensitized particle solution was taken and the volume measured. Further dialysis was carried out until the metal-to-ligand charge transfer (MLCT) absorbance at ~ 460 nm no longer changed (accounting for any volume change that had taken place). The Ru/Ir ratio of the retained colloid was estimated from the background corrected MLCT absorbance of the colloidal solution, with the assumption that all of the Ir was retained during dialysis. To remove excess Na_2SO_4, the solution was then dialyzed against 2 L of deionized water. Sensitized colloids were stored in the dark.

Particle Characterization. TEM samples were prepared by placing a drop of IrO_2 colloidal solution onto a copper grid (400 hexagonal mesh; carbon-coated Formvar). TEM images were obtained on a JEOL JEM 1200 EXII electron microscope using an acceleration voltage of 80 kV. FT-IR spectra were obtained using a Varian FTS 7000 Series Spectrophotometer. Surfactant−IrO_2 powder samples for IR analysis were attained by gently blowing a N_2 stream over an aqueous particle solution followed by vacuum drying at 80 °C. UV−visible spectroscopy was performed using a HP 8452A diode array spectrophotometer. Spectra were obtained using either a Pyrex or quartz cuvette (either 1 cm or 0.2 cm path length). For near-IR spectroscopy, a Varian Cary 500 Scan UV−vis−NIR spectrophotometer was used. Steady-state fluorescence spectra were acquired using a Fluorolog Horiba Jobin Yvon fluorimeter and samples were purged with argon using a custom-built 1 cm cuvette equipped with a 24/40 opening for rubber septa.

Steady-State Oxygen Evolution. Photochemical water oxidation reactions were carried out by first placing 10 mL Sensitizer-IrO_2 solution (vide infra) in a 39 mL Pyrex tube sealed with a rubber septum and purging the sample with argon for 30 min. This tube was then placed in an outer Pyrex jacket equipped with an adjustable O-ring at the bottom and sealed at the top with a rubber septum. Argon was flowed through the outer jacket to prevent leakage of air into the Pyrex tube during the experiment and to allow aliquots of O_2/Ar that were removed to be replenished with equal volumes of argon. Samples (1 or 2 mL) of O_2/Ar were removed from the Pyrex tube during the photochemical reaction via a sample-lock syringe. The solution was constantly stirred during oxygen evolution. A long pass filter (either >450 nm or >475 nm) was placed between the light source and the sample.

For photochemical oxygen evolution involving organic-surfactant stabilized IrO_2 colloids, the reaction solutions were prepared by adding $[Ru(bpy)_3](PF_6)_2$ (~0.11 mM), Na_2SO_4 (50 mM), $Na_2S_2O_8$ (10 mM), and surfactant−IrO_2 (final concentration = 6.2×10^{-5} M) to 10 mL of Na_2SiF_6/$NaHCO_3$ buffer ($[Na_2SiF_6]$ = 37.5 mM). The buffer was prepared by adding enough $NaHCO_3$ to Na_2SiF_6 (aq) to achieve pH 5.8, and the solution was aged overnight. The light intensity for photochemical oxygen evolution was 125 mW/cm^2.

For photochemical oxygen evolution involving Ru−complex sensitized IrO_2 colloids, 5 mL of the sensitizer−IrO_2 solution was added to 5 mL of Na_2SiF_6/$NaHCO_3$ buffer and then $Na_2S_2O_8$ (s) was added to make the solution 1 M. For comparison with $[Ru(bpy)_3](PF_6)_2$/succinate−IrO_2, 5 mL of 1.4×10^{-4} M $[Ru(bpy)_3](PF_6)_2$ in Na_2SiF_6/$NaHCO_3$ buffer was added to 5 mL of 1.66 mM dialyzed succinate−IrO_2 colloid. The absorbance of the sensitizers in each case was 1.0 at λ_{max}. In order to produce approximately the same number of excited states per unit time in each sensitizer case, a >450 nm long-pass filter was used for $[Ru(bpy)_3](PF_6)_2$/succinate−IrO_2, whereas a >475 nm long-pass filter was used in the case of $[Ru(dcb)_2(bpy(CONHSA)_2)]^{6-}$−$IrO_2$ and $[Ru(dcb)_3]^{4-}$−IrO_2. Nevertheless, the integrated absorptances of the sensitizers in each case were not equal (off by less than a factor of 1.5). The light intensity for photochemical oxygen evolution was 24 mW/cm^2.

Transient Absorbance. Transient absorption measurements were acquired using 532 nm laser excitation from a Nd:YAG Spectra-Physics Quantum-Ray laser. The samples were protected from a 300 W Xe probe beam using a fast shutter and appropriate UV/visible light filters. The probe light was positioned normal to the laser excitation beam and focused onto the sample. The transmitted light was then refocused on the entrance slit of a monochromator (Oriel) and detected using a photomultiplier tube (Products for Research, Inc.). Each kinetic trace was acquired by averaging 10−40 laser shots at a repetition rate of ~0.5 Hz. Samples were purged with argon for at least 15 min prior to flash photolysis studies. For samples containing sodium persulfate, band-pass filters (~450 nm) were placed before and after the sample holder.

Results and Discussion

Organic Surfactant Stabilized IrO_2 Nanoparticles. Previous literature reports involving surfactant-stabilized IrO_2 nanoparticles have exclusively used citrate as the surfactant to control particle growth and size.[29] In previous reports from this laboratory, a 4 h synthetic process using $pH_{initial}$ 7.5 was used to give citrate-stabilized nanoparticles that appear as large aggregates (>100 nm) of ~15 nm particles by TEM.[19,29] The synthesis in the current report was adjusted to allow for shorter reaction times (typically <20 min) by using a higher initial pH (=10). Under these conditions, comparable particle sizes and oxygen evolution rates were obtained using citrate. Upon closer examination by TEM, it was apparent that the ~15 nm particles themselves were aggregates of even smaller particles (Figure 1a). It was hypothesized that this smaller scale aggregation was caused by the third carboxylate group of citrate, which most likely orients itself away from the IrO_2 surface while the remaining two carboxylates bind to the surface. The third carboxylate group likely induces aggregation by binding to adjacent IrO_2 particles. This hypothesis was first tested by switching to the dicarboxylate surfactant, butylmalonate. Small, nonaggregated 2 nm particles were the result of this hydrothermal synthesis at 85−90 °C for <20 min (Figure 2c). A surfactant:Ir molar ratio of 60:1 was needed to achieve high yields of 2 nm particles with a low frequency of 10−20 nm aggregates. When a 6:1 ratio was used instead, a mixture of 2 nm particles and 10−20 nm aggregates resulted. Likewise, when the molar ratio of citrate:Ir was increased to 30:1, 2 nm particles formed; however, the particles existed as vast >100 nm aggregates, presumably due to the third carboxylate of citrate that allows for interparticle connections (Figure 1b).

Highly nonaggregated ~2 nm particles were also attained with less sterically bulky ligands like succinate and malonate (Figure 2, panels a and b). Interestingly, when acetate was used as the

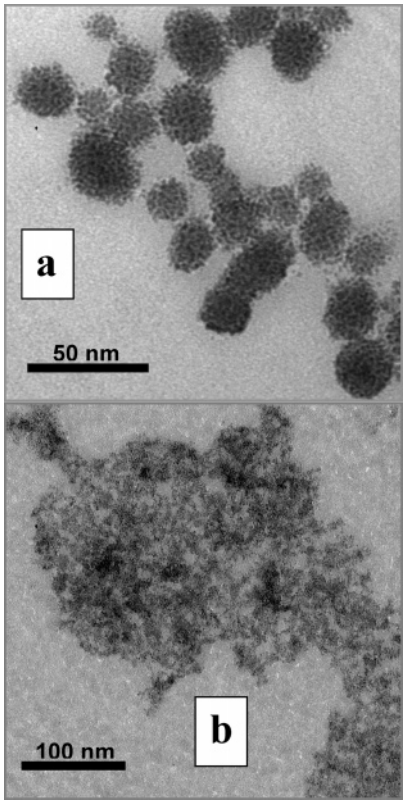

Figure 1. TEM images of IrO_2 nanoparticles synthesized with (a) 3:1 citrate:Ir molar ratio and (b) 30:1 citrate:Ir molar ratio.

surfactant, a molar ratio of 90:1 was needed to prevent obvious precipitation of IrO_2 solid during the hydrothermal synthesis. The particles obtained with 90:1 acetate appear as large >100 nm networks with primary 2 nm particles as the building block (Figure 2d). Similar results were observed with 60:1 phthalate:Ir but with highly fused networks of particles that were >200 nm (Figure 2e). The complete set of results for the synthesis of IrO_2 nanoparticles using organic surfactants is provided in Table 1. Importantly, aggregation was more prominent in all cases when the reaction temperature was ≥90 °C.

UV−visible spectroscopy was used to follow the course of the IrO_2 synthesis after rapidly cooling the colloidal solution to room temperature. The absorbance spectrum of IrO_2 colloids consists of an intense UV absorbance below 400 nm, a broad band with absorbance maximum at ∼550−700 nm that extends into the near-IR, and a nonzero baseline beyond 700 nm that is presumably a result of light scattering.[30] Interestingly, the wavelength of maximum absorbance for the broad visible band at ∼550−700 nm depended on the surfactant (Figure 3): butylmalonate (564 nm), succinate (572 nm), malonate (reaction time >15 min, 686 nm), and citrate (616 nm). Surfactants that provided predominantly small 2 nm particles produced either pink (30:1 citrate:Ir) or purple (e.g., BMA, malonate, and succinate at T <90 °C and t <15 min) colloidal solutions while larger (≥10 nm) particles gave blue colloidal solutions. In general, heating an aqueous solution of K_2IrCl_6 with the appropriate surfactant gives blue or purple solutions above 80−85 °C at reaction times less than 15 min. Continued heating of the colloids above 85−90 °C leads to an increase in absorbance beyond 700 nm, which is attributed to particle aggregation and enhanced light scattering.

Continued heating occasionally leads to an attenuation of the blue or purple color of the colloidal solution. In the case of 60:1 succinate:Ir, for instance, the reaction solution first turns

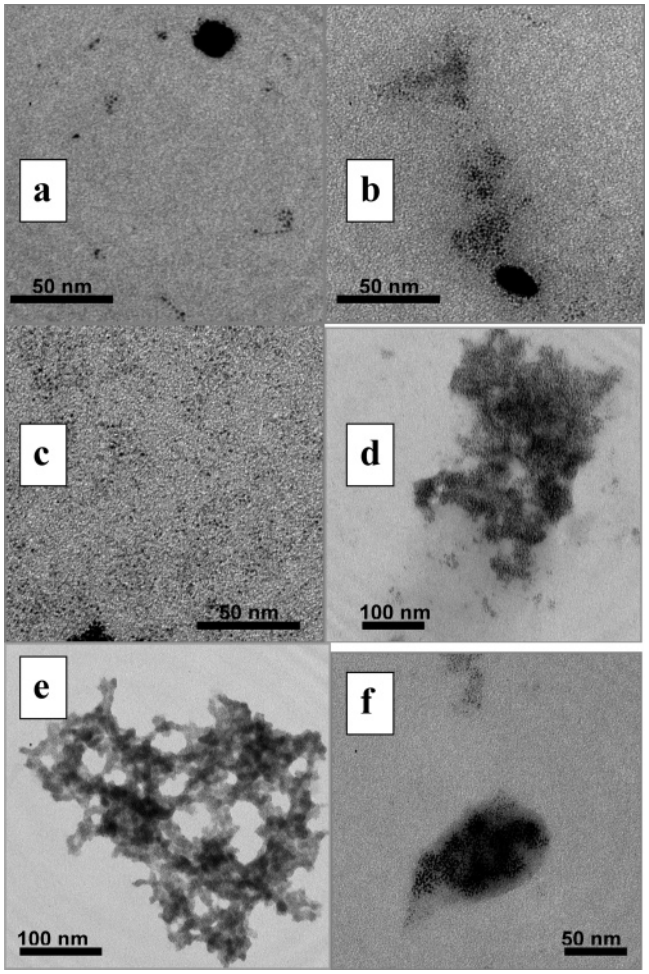

Figure 2. Organic surfactant-stabilized IrO_2 nanoparticles synthesized with (a) 60:1 succinate:Ir, (b) 6:1 malonate:Ir, (c) 60:1 butylmalonate:Ir, (d) 90:1 acetate:Ir, (e) 60:1 phthalate:Ir, and (f) 60:1 1-hydroxyethylidinediphosphonate:Ir.

purple above 85 °C and then green after several minutes of heating above 90 °C. The green color is indicative of Ir^{III} formation since blue or purple IrO_2 colloids turn green upon reduction by ascorbic acid.[30] The green color at elevated temperatures arises from oxidation of a solution species with concomitant reduction of Ir^{IV} to Ir^{III} based on the following observations. Rapid thermal quenching of the reaction solution using an ice−H_2O bath preserves the green color. In contrast, slow cooling of the reaction solution to room-temperature eventually restores the purple color. The rapidly quenched solution only returns to purple again after standing at room temperature for several minutes. Steady-state UV−visible spectra showed the reappearance of the band at ∼570 nm over time at room temperature. Presumably, the Ir^{III} that is formed during the high-temperature synthesis is reoxidized by a thermally activated electron-transfer process with dioxygen. Indeed, previous literature reports on IrO_2 colloids have shown that the particles exist as a mixed valence Ir^{III} and Ir^{IV}.[31] The absorbance band of IrO_2 in the visible is attributed to a d−d transition rather than an Ir^{III}/Ir^{IV} intervalence charge transfer since the band disappears upon reduction (all Ir^{III}) and gains intensity upon oxidation (presumably all Ir^{IV}).

UV−visible spectroscopy was also used to compare the particle growth kinetics for succinate and malonate ligands (see the Supporting Information). At a molar ratio of 60:1, particle growth with malonate is much slower than with succinate. The reaction solution for malonate remains yellow in color and never

TABLE 1: Results for IrO_2 Nanoparticle Synthesis Using Various Organic Surfactants[a]

surfactant	*n*	surfactant:Ir molar ratio	appearance (room temp, post heating)	TEM results
acetate		9:1	deep blue w/precipitate	microparticles
		90:1	deep blue	networks of aggregated 2 nm particles
citrate	2	3:1	blue	aggregates of 15 nm particles (Figure 1a)
		30:1	pink	>100 nm networks of 2 nm particles (Figure 1b)
butylmalonate	1	6:1	blue	2 nm particles + 10−20 nm aggregates of 2 nm particles
		60:1	purple	2 nm particles (Figure 2c)
		600:1	clear	
malonate	1	6:1	blue	2 nm particles + 10−20 nm aggregates of 2 nm particles
		10:1	purple	same as 6:1 (Figure 2b)
		60:1	yellow	
succinate	2	6:1	blue	2 nm particles + 10−20 nm aggregates of 2 nm particles
		60:1	purple	same as 6:1 (Figure 2a)
glutarate	3	6:1	blue	
		60:1	light purple	>100 nm networks of aggregated 2 nm particles
phthalate	2	6:1	blue-green	
		60:1	blue	>100 nm highly fused networks of particles (Figure 2e)
1−hydroxyethylidene−diphosphonate	1	6:1	blue−gray	
		60:1	blue−gray	>100 nm networks of aggregated 2 nm particles (Figure 2f)
1,2−phenylene−diphosphonate	2	6:1	blue−green	
		60:1	bright blue	
$[bpy(CONHMA)_2](Na)_4$	1	10:1	orange	

[a] *n* is the number of carbon atoms between two surface attachment groups.

TABLE 2: Results for IrO_2 Nanoparticle Synthesis in the Presence of Various Ruthenium(II) Sensitizers

surfactant	Ru:Ir molar ratio	reflux time (h)	appearance after dialysis	TEM results
$[Ru(bpy)_2(dcb)]^0$	5:1	1	precipitate formation during reflux	
$[Ru(bpy)(dcb)_2]^{2-}$	5:1	1	precipitate formation after dialysis	microparticles + 2 nm particles
$[Ru(dcb)_3]^{4-}$	5:1		red−brown colloidal solution	Figure S5
$[Ru(bpy)_2(dpbpy)]^{2-}$	10:1	1	precipitate formation during reflux	
$[Ru(dpbpy)_3]$	5:1	1, 16.5	blue−green colloidal solution	aggregates of 15 nm particles (Figure 4b)
$[Ru(bpy)_2(bpy(CONHMA)_2)](Na)_2$	5:1	1	Red colloid with precipitate	
$[Ru(bpy)_2(bpy(CONHSA)_2)](Na)_2$	5:1	1, 16.5	red colloid with precipitate	Figure 4a
$[Ru(dpbpy)_2(bpy(CONHMA)_2)]^{10-}$	5:1	1	red colloidal solution	2 nm particles + 10−20 nm aggregates
$[Ru(dpbpy)_2(bpy(CONHSA)_2)]^{10-}$	5:1	1	red colloidal solution	2 nm particles + 10−20 nm aggregates
$[Ru(dcb)_2(bpy(CONHSA)_2)]^{6-}$	1:1	16.5	red colloidal solution	Figure 4c
	5:1	1−50		Figure 6

turns the expected purple. Meanwhile, the purple color for succinate is achieved within a few minutes and continues to increase in intensity over time. In order to observe appreciable particle growth with malonate, the molar ratio needed to be lowered to ≤10:1 malonate:Ir. In the case of butylmalonate, the reaction solution remains colorless at a molar ratio of 600:1 but not at ≤60:1. Interestingly, when the initial pH is kept at 4 for 60:1 butylmalonate:Ir, purple solutions are not obtained even after 1 h of heating above 85 °C, and the reaction solution maintains a yellow hue.

Two surfactants containing diphosphonate groups were also explored for controlling IrO_2 nanoparticle growth: 1-hydroxyethanediphosphonate ($n = 1$) and 1,2-phenylenediphosphonate ($n = 2$), where *n* is the number of carbon atoms between surface attachment moieties (Table 1). At low surfactant:Ir ratios (<10:1 surfactant:Ir), the reaction solution contained both colloid as well as larger particles that precipitate out of solution. In stark contrast, the only carboxylated surfactant that gave obvious precipitation at short reaction times (<10 min) was acetate when a low 9:1 molar ratio was used. When phosphonates were used with 60:1 molar ratios, stable colloids were obtained without precipitate formation. However, TEM shows that the particles are highly flocculated networks of elementary 2 nm particles (Figure 2f). In general, particles synthesized with phosphonated surfactants were more highly aggregated than their carboxylated counterparts and failed to provide individual 2 nm particles.

Infrared spectroscopy was used to investigate the nature of the bonding between the surfactant and IrO_2. The interaction of the succinate ligand with the colloid surface was probed by first removing unbound succinate by extended dialysis and then removing the water to give a dry IrO_2 powder. The IR spectrum of well-dialyzed particles shows clear shifts to lower energy for both the asymmetric (1568−1558 cm^{-1}) and symmetric carboxylate stretches (1437−1400 cm^{-1}) (see the Supporting Information). These shifts are indicative of chemisorption of both carboxylate groups to the IrO_2 surface. The IR spectra also

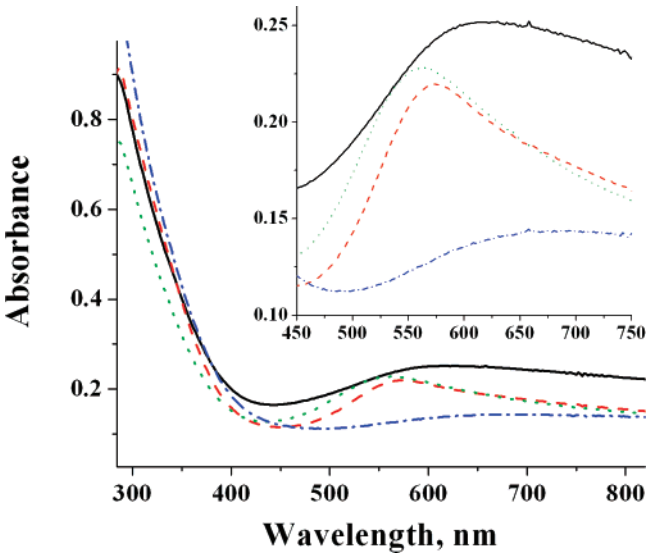

Figure 3. UV−vis absorbance spectra of IrO_2 nanoparticles stabilized with different organic surfactants: citrate (black solid line), succinate (red dashed line), butylmalonate (green dotted line), and malonate (blue dashed-dotted line). The inset zooms in on the broad visible absorbance band of the IrO_2 nanoparticles.

show that the surfactant remains fastened to IrO_2 even after exhaustive dialysis.

Photochemical oxygen evolution was examined for dicarboxylate-stabilized IrO_2 colloids and compared with citrate-stabilized IrO_2 colloids. Oxygen evolution was evident in all cases with similar oxygen evolution rates, suggesting that smaller 2 nm particle have similar activities for catalyzing for water oxidation. In previous studies, the photosensitizer of choice for the photochemical cycle has been exclusively $[Ru(bpy)_3](Cl)_2$.[30,32−34] Switching to the PF_6 salt slowed down the appearance of the plateau in oxygen evolution plots resulting in higher oxygen evolution yields. This observation was attributed to slower photosensitizer decomposition as supported by UV−visible spectroscopic data. The rate of decomposition for $[Ru(bpy)_3](PF_6)_2$ (1.2×10^{-4} s^{-1}) was 1 order of magnitude slower than that for $[Ru(bpy)_3](Cl)_2$ (7.1×10^{-3} s^{-1}), possibly a result of the lower solubility of $[Ru(bpy)_3](PF_6)_2$ in aqueous environments.

Sensitized IrO_2 Nanoparticles. In previous studies from our laboratory, it was hypothesized that the rate-limiting step of the photochemical oxygen evolution cycle was electron transfer from IrO_2 to the oxidized sensitizer. This hypothesis was supported by time-resolved UV−visible spectroscopic experiments examining electron transfer between IrO_2 and $[Ru(bpy)_3]^{3+}$ as well as kinetic isotope experiments showing that oxygen evolution rates were the same in H_2O and D_2O.[19] Tethering a sensitizer to the IrO_2 surface and then determining the kinetics of electron transfer using flash photolysis/transient absorbance methods allows us to examine this hypothesis without the complications of sensitizer diffusion, adsorption, and desorption. In addition, coupling sensitizers to the IrO_2 surface could lead to catalytic nanoparticles that can be integrated into potential visible light water-splitting systems in which the distance between excited-state electron acceptor (e.g., a wide band gap oxide semiconductor particle) and the water oxidation catalyst can be controlled precisely.

Three methods for "gluing" sensitizer molecules to IrO_2 nanoparticles were considered: (1) Chemisorption of sensitizers directly to the IrO_2 surface via displacement, (2) capping IrO_2 particles with surfactants having reactive groups for coupling to a sensitizer in a second step, and (3) IrO_2 nanoparticle synthesis in the presence of ruthenium sensitizer surfactants. Method 1 was attempted by heating $[Ru(dcb)_2(bpy(CONHSA)_2)]^{6-}$ (Chart 1, vide infra) with succinate-stabilized IrO_2 colloid at reflux for 16.5 h at a Ru:Ir molar ratio of 5:1. After prolonged dialysis, it was found that only a small portion of the Ru sensitizer had successfully displaced surface-bound succinate; the final ruthenium-to-iridium ([Ru]/[Ir]) concentration ratio was only 0.01. This experiment shows that the exchange kinetics are extremely slow and that surface-bound species on IrO_2 are difficult to displace, perhaps owing to the larger size of the Ru sensitizer surfactant ($R \sim 0.75$ nm) relative to the bound organic surfactant ($R \sim 0.17$ nm). Method 2 was attempted by heating K_2IrCl_6 in the presence of a bipyridine ligand functionalized with two malonate groups, $(bpy(CONHMA)_2)$. The goal was to provide pendant bipyridine ligands that are pre-fastened to the IrO_2 surface via the malonate groups and then couple the bipyridine ligands to $Ru(LL)_2Cl_2$ compounds to complete the sensitization process. The result was an orange solution reminiscent of $Ir(bpy)_n$ compounds and indicative of bidentate ligation to Ir metal centers via the bipyridine nitrogens.[35,36] Alternate strategies for forming linkages between capped nanoparticles and sensitizers will likely form either unstable bonds under aqueous conditions (e.g., ester), require reactants that are unstable in the presence of water (e.g., acyl chlorides), or require reaction conditions that may be deleterious to the catalytic activity of IrO_2 nanoparticles.

CHART 1: Dicarboxylic Acid Bipyridine (bpy(CONH-DCA)$_2$) Ligands with Malonate (MA) and Succinate (SA) Groups

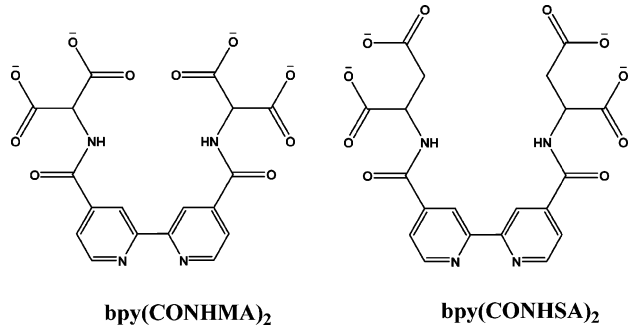

$bpy(CONHMA)_2$ $bpy(CONHSA)_2$

The method for sensitizing IrO_2 that remains is to synthesize the nanoparticles in the presence of sensitizers having the appropriate surface attachment chemistries. Ruthenium polypyridyl sensitizers were chosen to probe this possibility since they are thermally stable well above 100 °C, their electrochemical/photophysical properties can be easily tuned by altering ligands/ligand substituents,[37] and ligands having carboxylate and phosphonate surface attachment chemistries are easily attainable using known ligand syntheses from the literature. To begin probing this methodology, the ligands 4,4′-dicarboxylic acid-2,2′-bipyridine ($dcbH_2$) and 4,4′-diphosphonic acid-2,2′-bipyridine (dpbpy) were synthesized to prepare several heteroleptic ($[Ru(LL)_2(LL')]$) and homoleptic ($[Ru(LL)_3]$) ruthenium polypyridyl compounds. Because 2 nm IrO_2 particles could be stabilized by malonate and succinate, bipyridine ligands containing these dicarboxylate moieties, $bpy(CONHMA(OEt)_2)_2$ and $bpy(CONHSA(OMe)_2)_2)$, were synthesized by coupling 4,4′-dicarbonyl chloride-2,2′-bipyridine with the appropriate esterified amino acid derivative. These ligands were reacted with $Ru(LL)_2(Cl)_2$ to give the desired ruthenium(II) heteroleptic compounds, $[Ru(LL)_2(bpy(CONHSA(OMe)_2)_2)]$ and $[Ru(LL)_2(bpy(CONHMA(OEt)_2)_2)]$, which were then saponified to give the carboxylated derivatives.

CHART 2: Ruthenium(II) Polypyridyl Compounds Used for Synthesizing Sensitized IrO_2 Nanoparticles

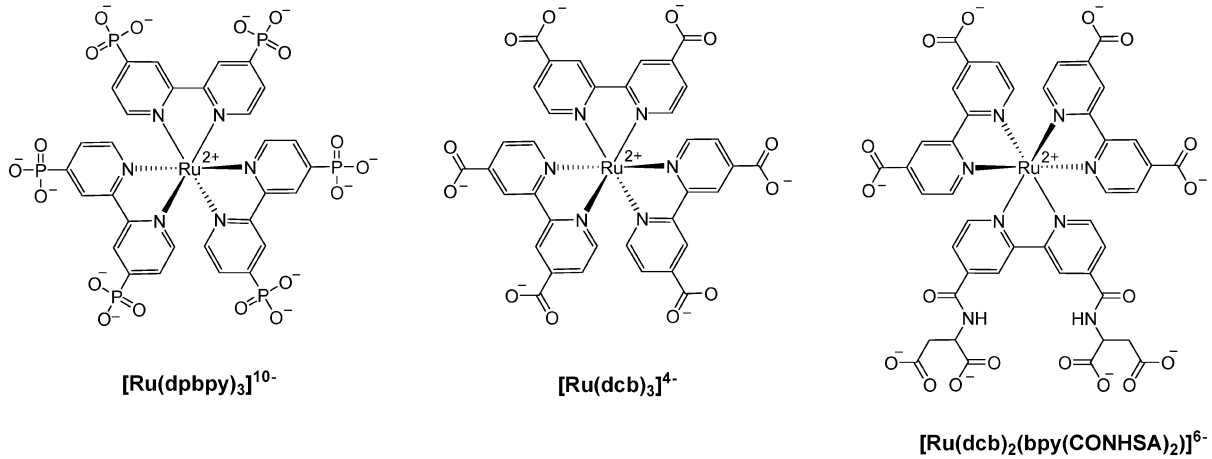

In order to synthesize sensitized IrO_2 colloids, K_2IrCl_6 was heated in the presence of sensitizer "surfactants" at $pH_{initial}$ 10. The colloidal solution was then exhaustively dialyzed to remove unbound sensitizers leaving behind sensitized particles. A series of control experiments showed that complete elution through the dialysis membranes was possible for each Ru compound in the absence of IrO_2, leaving behind clear solutions. For the heteroleptic compounds, $[Ru(bpy)_2(dpbpy)]^{2-}$ and $[Ru(bpy)_2(dcb)]^0$ (5:1 Ru:Ir molar ratio), a precipitate was evident after refluxing for 1−2 min and was more prominent in the case of $[Ru(bpy)_2(dcb)]^0$. According to TEM images, $[Ru(bpy)(dcb)_2]^{2-}$ (5:1 Ru:Ir molar ratio) gave a mixture of 2 nm IrO_2 particles and large microparticles. In contrast, both $[Ru(dpbpy)_3]^{10-}$ and $[Ru(dcb)_3]^{4-}$ (5:1 Ru:Ir, 16.5 h reflux) produced stable colloidal solutions before and after extended dialysis was performed to remove unbound sensitizers. TEM measurements showed that $[Ru(dpbpy)_3]^{10-}$ gave clusters of ∼15 nm particles reminiscent of those produced in the presence of 3:1 citrate:IrO_2 (Figure 4b). In contrast, $[Ru(dcb)_3]^{4-}$ gave primarily 2 nm particles with occasional ∼10−20 nm aggregates of 2 nm particles. Consistent with the relative particle sizes, the [Ru]/[Ir] ratio for $[Ru(dpbpy)_3]-IrO_2$ particles was 0.021, whereas that for $[Ru(dcb)_3]-IrO_2$ was 1 order of magnitude larger (0.12). The fact that $[Ru(dcb)_3]^{4-}$ is able to stabilize 2 nm particles suggests either a steric effect, a charge effect, or a combination of both.

For complexes in which LL = dcb or dpbpy and LL′ = bpy(CONHMA)$_2$ or bpy(CONHSA)$_2$, a 1-h reflux at 5:1 Ru:Ir molar ratio leads to the production of 2 nm particles with a minor fraction of larger 10−20 nm aggregates of the 2 nm particles. Interestingly, when LL is bipyridine, the IrO_2 particles appear as larger (>200 nm) networks of particles with no signs of elementary 2 nm particles (Figure 4a). The additional anionic charge provided by ancillary ligands dcb and dpbpy appears to prevent aggregation of the 2 nm primary particles.

In order to optimize the extent of sensitization for the sensitized IrO_2 colloids, both the temperature and time dependence were examined. Initial temperature studies performed using $[Ru(dcb)_2(bpy(CONHSA)_2)]^{6-}$ showed that higher temperatures (i.e., reflux) and longer reaction times (6.5 vs 1.0 h) gave higher [Ru]/[Ir] values. Based on these results, the remainder of the reaction time experiments was performed at reflux temperature. Figure 5 shows reaction time data for three different sensitizers: $[Ru(dcb)_2(bpy(CONHSA)_2)]^{6-}$, $[Ru(dcb)_3]^{4-}$, and $[Ru(dpbpy)_3]^{10-}$. This data provides several insights. First, it shows that the binding strength of the complexes follows the order $[Ru(dcb)_2(bpy(CONHSA)_2)]^{6-} > [Ru(dcb)_3]^{4-} \gg [Ru(dpbpy)_3]^{10-}$. Since $[Ru(dpbpy)_3]^{10-}$ gives particles that are ∼7 times larger than those observed with $[Ru(dcb)_2(bpy(CONHSA)_2)]^{6-}$ or $[Ru(dcb)_3]^{4-}$, it can be inferred that particle growth is faster in the presence of phosphonates due to weaker interactions with the IrO_2 surface. Second, replacing a dcb ligand with bpy(CONHSA)$_2$ apparently increases surface adsorption by a factor of 1.5, strongly suggesting that dicarboxylate ligands such as malonate and succinate bind more strongly to IrO_2 surfaces than do monocarboxylates. Although dcb ligands can bind to the IrO_2 surface through their carboxylate groups, it is important to note that simultaneous binding by the carboxylate groups of bpy(CONHSA)$_2$ and dcb is geometrically unlikely for $[Ru(dcb)_2(bpy(CONHSA)_2)]^{6-}$.

The time-dependent sensitization experiments were also examined by TEM. For both $[Ru(dcb)_2(bpy(CONHSA)_2)]^{6-}$ and $[Ru(dcb)_3]^{4-}$, it was apparent that sensitized IrO_2 colloids have two distinguishable growth stages: deaggregation followed by reaggregation (Figure 6). At short reaction times (<6.5 h), the particles appear as small clusters of 2 nm particles which tend to break apart into nonaggregated particles between 6.5 and 16.5 h. Over time (>16.5 h), the particles appear to reaggregate into extended clusters of 2 nm particles. One possible explanation for this is that the strength of the sensitizer−IrO_2 interaction plateaus between 6.5 and 16.5 h causing the break up of the initially formed clusters. The subsequent reaggregation is then a result of interparticle bridging caused by the carboxylate groups on the ancillary bpy ligands.

Since 5:1 Ru:Ir molar ratios require fairly large amounts of Ru sensitizer starting material (typically 10−100 mg), it is advantageous to consider smaller molar ratios. To this end, a Ru:Ir molar ratio of 1:1 was chosen for $[Ru(dcb)_2(bpy(CONHSA)_2)]^{6-}$ using reflux temperature for 16.5 h. Compared to TEM images for 5:1 Ru:Ir molar ratio under identical conditions, the 1:1 molar ratio showed a larger yield of small ∼10 nm aggregates of 2 nm particles (Figure 4c). These data suggest that higher molar ratios may be needed to prevent the formation of larger aggregates.

Spectroscopic Characterization of Sensitized IrO_2 Particles. Sensitized IrO_2 nanoparticles were characterized using steady-state and time-resolved absorption and emission spectroscopy. Figure 7 shows normalized UV−vis spectra for $[Ru(dcb)_2(bpy(CONHSA)_2)]^{6-}-IrO_2$ colloids overlaid with the spectrum for unbound $[Ru(dcb)_2(bpy(CONHSA)_2)]^{6-}$. There is an increased scattering background for the sensitized colloids. The intensity of the absorbance beyond 700 nm reaches a minimum at 16.5 h (Figure 7, inset) consistent with the

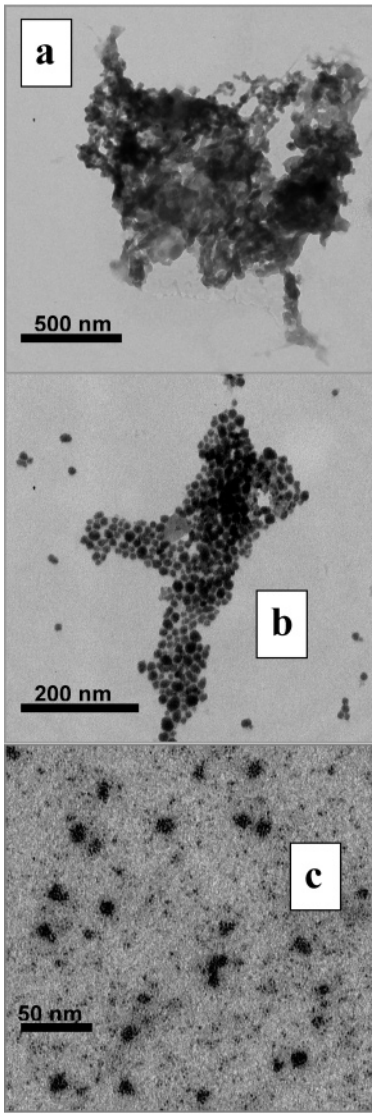

Figure 4. TEM images of (a) $[Ru(bpy)_2(bpy(CONHSA)_2)]^{6-}-IrO_2$ (5:1 Ru:Ir, 18 h reflux), (b) $[Ru(dpbpy)_3)]^{10-}-IrO_2$ (5:1 Ru:Ir, 16.5 h reflux), and (c) $[Ru(dcb)_2(bpy(CONHSA)_2)]^{6-}-IrO_2$ (1:1 Ru:Ir, 16.5 h reflux).

deaggregation/reaggregation mechanism proposed above and its anticipated effect on light scattering.

Photoluminescence spectroscopy was used to study quenching of the MLCT excited-state by IrO_2 colloids for $[Ru(dcb)_2(bpy(CONHSA)_2)]^{6-}$, $[Ru(dcb)_3]^{4-}$, and $[Ru(dpbpy)_3]^{10-}$. Photoluminescence spectra were recorded for each of the reaction times shown in Figure 5 following extensive dialysis and compared with that for the unbound sensitizers. In each case, the photoluminescence of the unbound sensitizer was quenched by ≥95% upon adsorption to the IrO_2 surface.[38,39] Interestingly, the exchange reaction between $[Ru(dcb)_2(bpy(CONHSA)_2)]^{6-}$ and succinate$-IrO_2$ to give sensitized colloids also showed considerable photoluminescence quenching (99%). This shows that the dialysis procedure effectively removes unbound Ru sensitizers leaving behind the desired sensitized particles. The excited-state quenching mechanism involves either oxidative or reductive electron transfer to/from IrO_2. Transient absorbance experiments involving $[Ru(dcb)_2(bpy(CONHSA)_2)]^{6-}-IrO_2$ showed a very weak negative ΔA at 450 nm, consistent with formation of Ru^{III} via excited-state electron transfer to IrO_2 and previous studies by Resch and Fox involving porphyrin-capped RuO_2 particles.[38] Reductive quenching would be expected to give a positive ΔA at 450 nm based on photolysis experiments

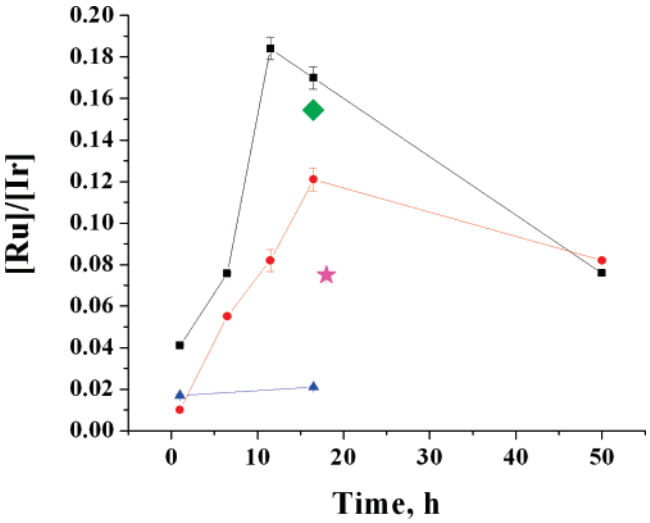

Figure 5. Extent of sensitization versus time for three different sensitizers; colloids were synthesized at reflux temperature with a Ru:Ir molar ratio of 5:1: $[Ru(dcb)_2(bpy(CONHSA)_2)]^{6-}-IrO_2$ (black line with squares), $[Ru(dcb)_3]^{4-}-IrO_2$ (red line with circles), and $[Ru(dpbpy)_3]^{10-}-IrO_2$ (blue line with triangles). The green diamond data point corresponds to a 16.5 h reaction involving $[Ru(dcb)_2(bpy(CONHSA)_2)]^{6-}-IrO_2$ using a 1:1 Ru:Ir molar ratio. The magenta star corresponds to an 18 h reaction involving $[Ru(bpy)_2(bpy(CONHSA)_2)]^{2-}-IrO_2$ using a 5:1 Ru:Ir molar ratio.

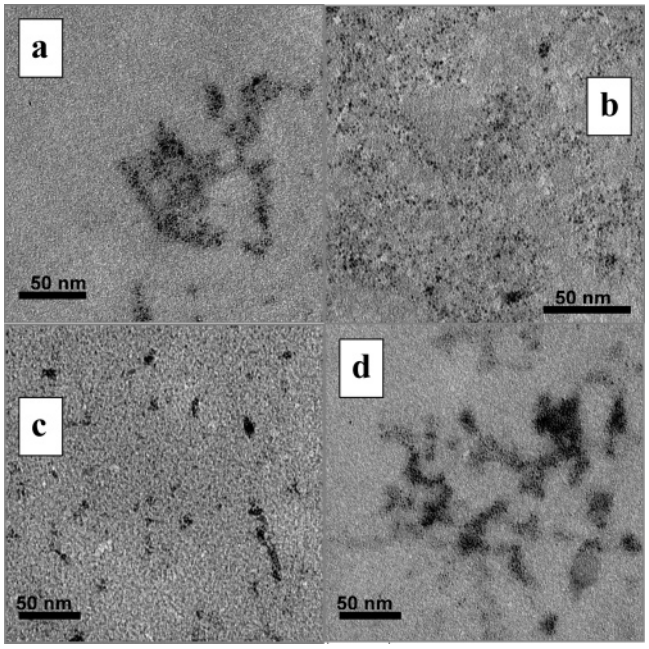

Figure 6. TEM images of $[Ru(dcb)_2(bpy(CONHSA)_2)]^{6-}-IrO_2$ taken after (a) 1, (b) 6.5, (c) 16.5, and (d) 50 h of reflux.

performed with $[Ru(bpy)_2(bpy(CONHSA)_2)]^{2-}$ in the presence of triethylamine in acetonitrile. The extinction coefficient of IrO_2 is at least 1 order of magnitude less than that of the Ru(II) MLCT absorbance and therefore should contribute negligibly to the observed ΔA.

The rate constant for excited-state electron transfer to IrO_2 was calculated to be $\sim 3.0 \times 10^7$ s^{-1} for $[Ru(dcb)_2(bpy(CONHSA)_2)]^{6-}-IrO_2$ and $[Ru(dcb)_3]^{4-}-IrO_2$ using the following equation:[38]

$$k_{ET} = \frac{(\phi_{PL}^0/\phi_{PL}) - 1}{\tau_{PL}^0} \approx k_D^0\left[\frac{I_0}{I} - 1\right]$$

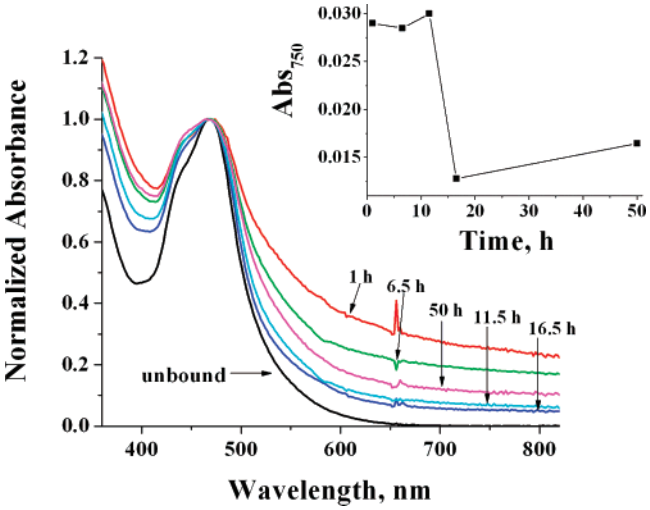

Figure 7. Normalized UV−vis absorbance spectra for $[Ru(dcb)_2(bpy(CONHSA)_2)]^{6-}$−$IrO_2$ (5:1 Ru:Ir molar ratio) after different reaction times compared with unbound $[Ru(dcb)_2(bpy(CONHSA)_2)]^{6-}$ sensitizer: unbound (black line), 1 (red line), 6.5 (green line), 11.5 (blue line), 16.5 (cyan line), and 50 h (magenta line). Inset: Absorbance (not normalized) at 750 nm plotted against reaction time.

where

$$k_D^0 = (\tau_{PL}^0)^{-1} \quad (1)$$

where ϕ_{PL}^0 is the quantum yield for photoluminescence in the absence of quencher and ϕ_{PL} is the quantum yield for photoluminescence in the presence of quencher. The excited-state lifetimes in the absence of IrO_2, τ_{PL}^0, for $[Ru(dcb)_2(bpy(CONHSA)_2)]^{6-}$, $[Ru(dcb)_3]^{4-}$, and $[Ru(bpy)_3](PF_6)_2$ were determined to be 560, 710, and 620 ns, respectively, by time-resolved photoluminescence (see the Supporting Information).

At the sensitizer and IrO_2 nanoparticle concentrations used in oxygen evolution experiments, excited-state quenching of unbound $[Ru(dcb)_2(bpy(CONHSA)_2)]^{6-}$ by succinate-capped IrO_2 nanoparticles is negligible. Contact between the redox partners is inhibited by electrostatic repulsion between the anionic sensitizer molecules and anionic succinate−IrO_2 nanoparticles at pH 7. The lack of excited-state quenching also suggests that adsorption of sensitizer molecules to the IrO_2 surface via carboxylate groups is negligible at room temperature. In contrast, the photoluminescence of cationic $[Ru(bpy)_3](PF_6)_2$ is considerably quenched at succinate−IrO_2 concentrations above 0.5 mM. Stern−Volmer analysis (see the Supporting Information) shows that the extent of quenching plateaus above 1 mM IrO_2 concentration, consistent with adsorption of the sensitizer at the colloid surface. Interestingly, the extent of excited-state quenching of $[Ru(bpy)_3](PF_6)_2$ by IrO_2 falls to ∼10% in the presence of $Na_2SiF_6/NaHCO_3$, suggesting that adsorption of the cationic sensitizer to negatively charged silica particles (the result of Na_2SiF_6 hydrolysis) competes with adsorption onto IrO_2.

Transient absorbance spectroscopy was used to study the kinetics of electron transfer between the oxidized sensitizer and IrO_2 for both bound and unbound cases (Figures 9 and 10). Flash photolysis experiments were performed in the presence of sodium persulfate to form the oxidized sensitizer in situ and monitor its disappearance. Since the solutions were photoactive, care was taken to handle samples in the dark and minimize steady-state UV−vis absorbance changes so that reliable data could be obtained. In the case of $[Ru(dcb)_2(bpy(CONHSA)_2)]^{6-}$−

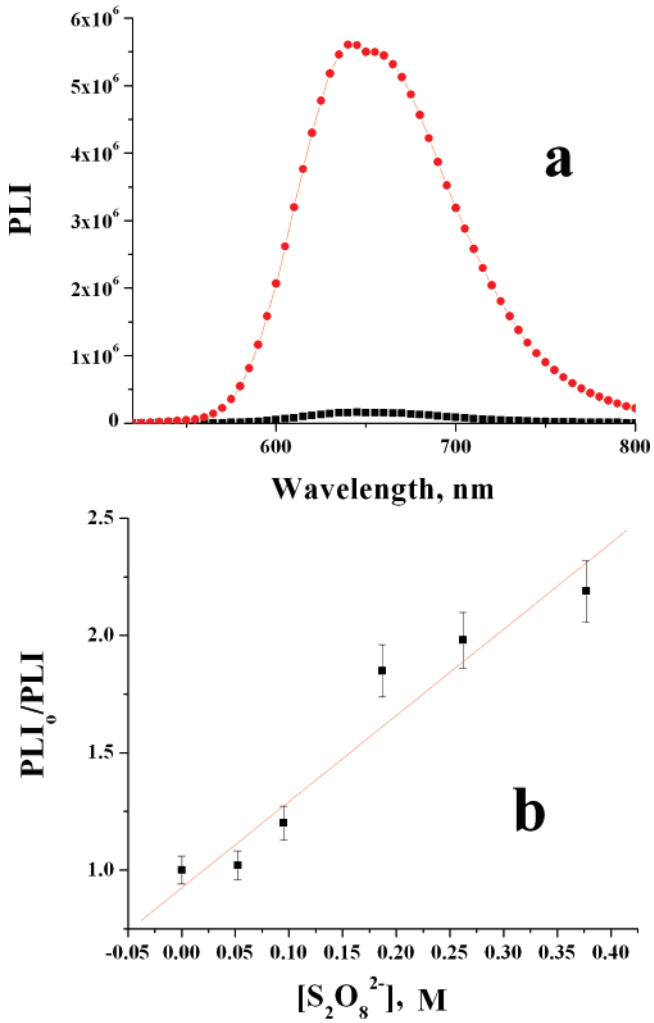

Figure 8. (a) Photoluminescence spectra measured in front-face mode for IrO_2 nanoparticles sensitized with $[Ru(dcb)_2(bpy(CONHSA)_2)]^{6-}$ (black line with squares) and unbound $[Ru(dcb)_2(bpy(CONHSA)_2)]^{6-}$ (red line with circles). The absorbance of the sensitizer at the excitation wavelength (470 nm) was approximately equal in the two spectra; the difference was accounted for in calculating the extent of quenching (97% in this case). Similar experiments were performed for all sensitizer-stabilized IrO_2 colloids after extended dialysis and showed >95% photoluminescence quenching. (b) Stern−Volmer plot for quenching of $[Ru(dcb)_2(bpy(CONHSA)_2)]^{6-}$−$IrO_2$ by persulfate in the presence of $Na_2SiF_6/NaHCO_3$ buffer.

IrO_2, bleaching recovery of Ru^{II} occurred via a pseudo first-order process with an observed rate constant, $k_{obs} = 8.0\ (\pm 0.3) \times 10^2\ s^{-1}$. With $[Ru(bpy)_2(bpy(CONHSA)_2)]^{2-}$−$IrO_2$, the bleaching recovery process was more complex, showing a major component with a first-order rate constant comparable to that of $[Ru(dcb)_2(bpy(CONHSA)_2)]^{6-}$−$IrO_2$ ($k_{obs} = \sim 8 \times 10^2\ s^{-1}$) and a longer lived component. Bleaching recovery of $[Ru(dcb)_3]^{4-}$−IrO_2 also followed pseudo-first-order kinetics with a slightly slower rate constant, $k_{obs} = 3.4\ (\pm 0.4) \times 10^2\ s^{-1}$. The observed rate constants for the sensitizer-stabilized IrO_2 colloids were, within experimental error, the same in the presence and absence of buffer. In contrast, the bleaching recovery kinetics for $[Ru(bpy)_3](PF_6)_2$/succinate−IrO_2 contained both slow and fast components. The fast component was pseudo-first-order, and k_{obs} increased from 5.2 (± 0.01) $\times 10^3\ s^{-1}$ to 1.7 (± 0.02) $\times 10^4\ s^{-1}$ when the succinate−IrO_2 concentration was increased from 0.42 to 0.83 mM in the presence of $Na_2SiF_6/NaHCO_3$.[40] The relative amplitude of the fast component depended on both the IrO_2 concentration and the presence of

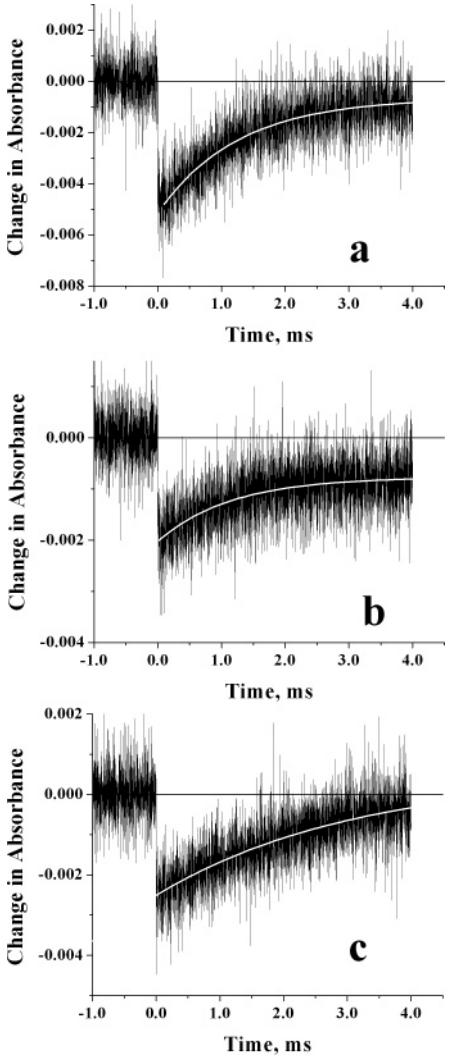

Figure 9. Single wavelength kinetic traces recorded at 450 nm following 532 nm, 10 ns laser excitation, showing the *in situ* formation and disappearance of Ru^{III}: (a) $[Ru(dcb)_2(bpy(CONHSA)_2)]^{6-}-IrO_2$ (16.5 h, 5:1 Ru:Ir molar ratio), $[IrO_2] = 0.48$ mM, $[NaS_2O_8] = 1$ M, (b) $[Ru(bpy)_2(bpy(CONHSA)_2)]^{2-}-IrO_2$ (18 h, 5:1 Ru:Ir molar ratio, $[IrO_2] = 0.46$ mM, $[NaS_2O_8] = 1$ M, and (c) $[Ru(dcb)_3]^{6-}-IrO_2$ (16.5 h, 5:1 Ru:Ir molar ratio, $[IrO_2] = 0.43$ mM, $[NaS_2O_8] = 1$ M. Overlaid white lines are fits to a first-order bleaching recovery process.

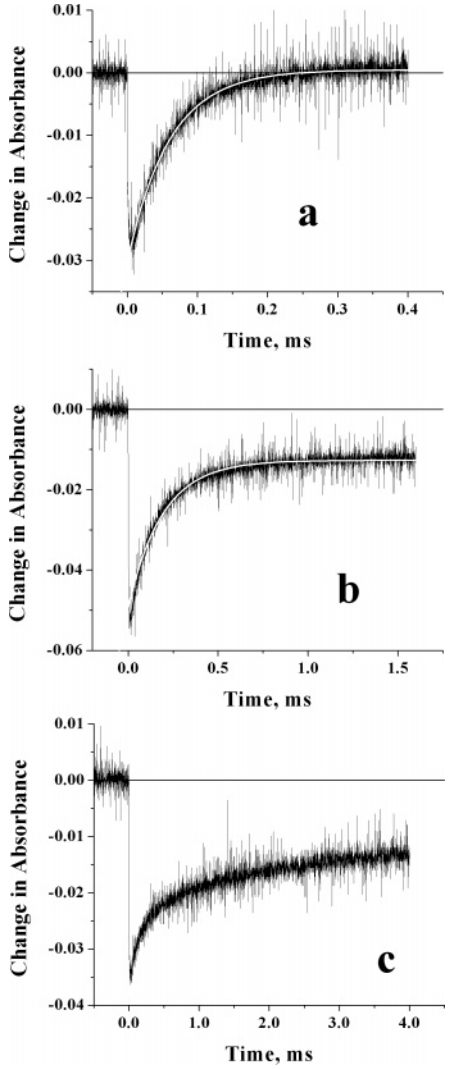

Figure 10. Single wavelength kinetics recorded at 450 nm following 532 nm, 10 ns laser excitation, showing in situ formation and disappearance of Ru^{III} for $[Ru(bpy)_3](PF_6)_2$ (0.057 mM), succinate$-IrO_2$, and $[NaS_2O_8] = 0.25$ M: (a) 0.83 mM succinate$-IrO_2$ with $Na_2SiF_6/NaHCO_3$ buffer, (b) 0.42 mM succinate$-IrO_2$ with $Na_2SiF_6/NaHCO_3$ buffer, and (c) 0.42 mM succinate$-IrO_2$ with no buffer. Overlaid white lines in panels a and b are fits to a first-order bleaching recovery process.

buffer, as shown in Figure 10. At high buffer and IrO_2 concentration, the fast first-order process was dominant, whereas at lower IrO_2 concentration, bleaching recovery was slow ($\gg$5 ms) and non-first-order. This trend is consistent with a fast, first-order electron transfer between IrO_2 and electrostatically adsorbed sensitizer molecules and a slower process involving nonadsorbed sensitizer molecules. The fact that the relative amplitude of the fast component depends on the presence of buffer can be explained by the formation of succinate$-IrO_2$/silica particle composites. The anionic silica support elevates the local concentration of $[Ru(bpy)_3]^{2+}$ at the IrO_2 nanoparticle surface, resulting in slightly faster kinetics and larger relative amplitudes for the fast component.[29] As expected, the kinetics of bleaching recovery were not affected by the presence of buffer in the case of the sensitized colloids (vide supra).

Photochemical Oxygen Evolution by Sensitized IrO_2 Particles. Steady-state photochemical oxygen evolution for the sensitized colloids was compared with the unbound $[Ru(bpy)_3]^{2+}$/succinate-stabilized IrO_2 system. Both solutions contained the same concentration of buffer, similar concentrations of IrO_2, and also the same concentration of the excited-state oxidant, sodium persulfate. The integrated ground-state absorptances for the sensitizers were fixed to within a factor of 1.5 by means of light filters with different cutoff wavelengths. Figure 11 shows that the oxygen evolution rate is approximately 2 times faster for $[Ru(bpy)_3]^{2+}$/succinate$-IrO_2$ (0.22 μmol/min) than it is for $[Ru(dcb)_2(bpy(CONHSA)_2)]^{6-}-IrO_2$ and $[Ru(dcb)_3]^{4-}-IrO_2$ (0.13 and 0.10 μmol/min, respectively). This result was initially surprising when one considers the rapid and efficient quenching of the MLCT excited-state by IrO_2 that occurs with the sensitized IrO_2 colloids. In order for oxygen to be produced, excited-state oxidative quenching by persulfate must be kinetically competitive with excited-state electron transfer to IrO_2. In order to understand the similar rates of oxygen evolution that were observed for the bound and unbound cases, excited-state quenching by persulfate was studied (Figures 8b and S8). The Stern$-$Volmer constants for persulfate quenching of the luminescence were 500 and 3.4 M^{-1} for $Ru(bpy)_3]^{2+}$/succinate$-IrO_2$ and $[Ru(dcb)_2(bpy(CONHSA)_2)]^{6-}-IrO_2$, respectively. Because the photoluminescence quantum yield is diminished

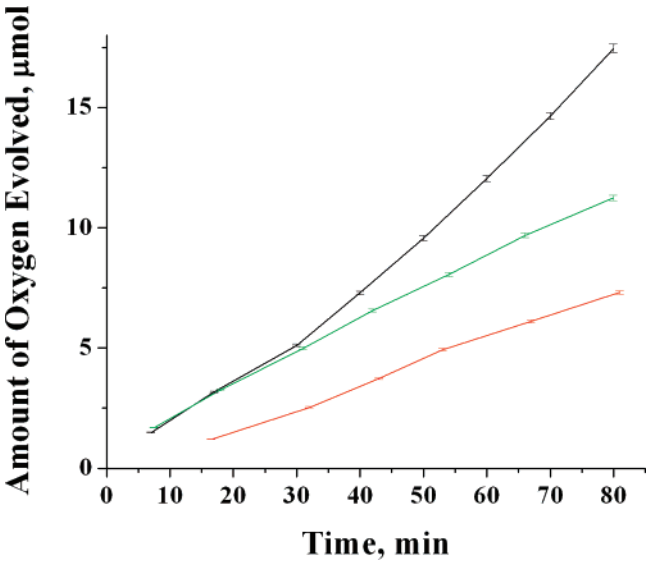

Figure 11. Photochemical oxygen evolution data for $[Ru(bpy)_3](PF_6)_2$/succinate−IrO_2 (black line), $[Ru(dcb)_3]^{4-}$−IrO_2 (red line), and $[Ru(dcb)_2(bpy(CONHSA)_2)]^{6-}$−$IrO_2$ (green line).

by 10% in the presence of IrO_2 and buffer for $[Ru(bpy)_3]^{2+}$, the excited-state lifetime in the absence of persulfate was taken to be (620 ns)(0.90) = 560 ns. For $[Ru(dcb)_2(bpy(CONHSA)_2)]^{6-}$−$IrO_2$, the excited-state lifetime in the absence of persulfate was estimated to be (560 ns)(0.05) = 28 ns.[41] Hence, the persulfate quenching rate constants, k_q, were calculated to be 8.8×10^8 and 1.2×10^8 M^{-1} s^{-1} for $[Ru(bpy)_3]^{2+}$/succinate−IrO_2 and $[Ru(dcb)_2(bpy(CONHSA)_2)]^{6-}$−$IrO_2$, respectively, and the time constants were 1.1 and 8.5 ns at a persulfate concentration of 1 M. Using the rate constants derived above for excited-state electron transfer to IrO_2, the time constants for this process are 227 and 33 ns for $[Ru(bpy)_3]^{2+}$/succinate−IrO_2 and $[Ru(dcb)_2(bpy(CONHSA)_2)]^{6-}$−$IrO_2$, respectively. According to this analysis, excited-state electron transfer from $[Ru(dcb)_2(bpy(SA)_2)]^{6-}$−$IrO_2$ to persulfate is faster than excited-state quenching by IrO_2 by a factor of 3.9. Excited-state quenching by persulfate (and therefore oxygen evolution) is more efficient in the more weakly coupled $[Ru(bpy)_3]^{2+}$/succinate−IrO_2 system because quenching by IrO_2 is an order of magnitude slower.

Using rate constants obtained from transient absorbance experiments, the second-order rate constants for reduction of the oxidized sensitizer by IrO_2 are 6.8×10^7, 4.0×10^6, and 1.9×10^6 M^{-1} s^{-1}, for $[Ru(bpy)_3](PF_6)_2$, $[Ru(dcb)_2(bpy(CONHSA)_2)]^{6-}$, and $[Ru(dcb)_3]^{4-}$, respectively. These rate constants are calculated on a per-surface atom basis, assuming that 42% of the Ir atoms in a 2 nm particle are on the surface. In a previous report from this laboratory, the second-order rate constant for the $[Ru(bpy)_3](Cl)_2$/citrate-stabilized IrO_2 system was found to be 3.0×10^6 M^{-1} s^{-1}.[19] This order of magnitude agreement is reasonable considering the differences in IrO_2 particle sizes (10−20 nm vs 2 nm), the different counterions used (Cl^- vs PF_6^-), and the time scale (>100 ms) of observations in our earlier experiments. The turnover numbers for photochemical oxygen evolution were determined to be 170, 149, and 117 for $[Ru(bpy)_3](PF_6)_2$, $[Ru(dcb)_2(bpy(CONHSA)_2)]^{6-}$, and $[Ru(dcb)_3]^{4-}$, respectively.

Conclusions

Bidentate carboxylate ligands containing malonate and succinate groups stabilize 2 nm diameter particles of catalytically active IrO_2. Control experiments with chemically related ligands (acetate and citrate) suggest that chelation of surface Ir atoms is an important factor in stabilizing these nanoparticles against aggregation. In the case of citrate, it appears that the third carboxylate group is responsible for aggregation of the primary 2 nm particles into larger aggregates. Phosphonate ligands do not stabilize the particles as well as carboxylate ligands. This finding may have useful implications for designing bifunctional sensitizer molecules that can bridge between oxide semiconductors (TiO_2, ZnO, Nb_2O_5, etc.), which tend to make good bonds to phosphonate ligands, and IrO_2 catalyst nanoparticles.

IrO_2 particles synthesized in the presence of succinate-capped ruthenium poly(pyridyl) sensitizer molecules are also stabilized against aggregation, and the bound sensitizer molecules are not removed by dialysis. The quenching of the excited-state of the bound sensitizer molecules on the 30 ns time scale is indicative of good electronic coupling between the sensitizer and IrO_2. Importantly, the excited-state of the bound sensitizer molecules can be quenched oxidatively by persulfate, in a process that is kinetically competitive with oxidative quenching of the tethered sensitizer by IrO_2. Under these conditions, oxygen evolution occurs. This finding is encouraging in terms of the ultimate incorporation of the sensitizer−IrO_2 diads into photochemical water splitting systems. Electron-transfer quenching of photoexcited ruthenium polypyridyl sensitizers by TiO_2, ZnO, and other oxide semiconductors is ordinarily a fast process that should be able to compete with quenching by IrO_2.[42,43] These rates should also vary with the length and electronic nature of the linkers between the sensitizer, the oxide, and the catalyst nanoparticles. In principle, these properties of the molecules and their effect on the quantum yield of charge separation and oxygen evolution can be studied systematically, now that a good set of ligands exists for stabilizing very small IrO_2 nanoparticles.

Acknowledgment. This work was supported by the Division of Chemical Sciences, Office of Basic Energy Sciences, U.S. Department of Energy under Contract DE-FG02-05ER15749. W.J.Y. thanks the Donors of the ACS Petroleum Research Fund for support of this research in the form of a postdoctoral fellowship.

Supporting Information Available: UV−visible and infrared spectra of complexes and sensitized IrO_2 particles. Photochemical oxygen evolution data for surfactant stabilized IrO_2 particles. Additional TEM images of sensitizer-stabilized colloids. Photoluminescence quenching data for sensitizer-IrO_2 systems. Photophysical properties of Ru(polypyridyl) sensitizers. This material is available free of charge via the Internet at http://pubs.acs.org.

References and Notes

(1) Bard, A. J.; Fox, M. A. *Acc. Chem. Res.* **1995**, *28*, 141−145.
(2) Asahi, R.; Mirokawa, T.; Ohwaki, T.; Aoki, K.; Taga, Y. *Science* **2001**, *293*, 269.
(3) Kasahara, A.; Nukumizu, K.; Takata, T.; Kondo, J. N.; Hara, M.; Kobayashi, H.; Domen, K. *J. Phys. Chem. B* **2003**, *107*, 791.
(4) Kasahara, A.; Nukumizu, K.; Hitoki, G.; Takata, T.; Kondo, J. N.; Hara, M.; Kobayashi, H.; Domen, K. *J. Phys. Chem. A* **2002**, *106*, 6750.
(5) Kim, H. G.; Hwang, D. W.; Lee, J. S. *J. Am. Chem. Soc.* **2004**, *126*, 8912−3.
(6) Kim, H. G.; Borse, P. H.; Choi, W.; Lee, J. S. *Angew. Chem., Int. Ed.* **2005**, *44*, 4585−9.
(7) Kim, H. G.; Jeong, E. D.; Borse, P. H.; Jeon, S.; Yong, K.; Lee, J. S.; Li, W.; Oh, S. H. *Appl. Phys. Lett.* **2006**, *89*, 64103.
(8) Zou, Z.; Ye, J.; Sayama, K.; Arakawa, H. *Nature* **2001**, *414*, 625.
(9) Maeda, K.; Teramura, K.; Takata, T.; Lu, Daling.; Saito, N.; Inoue, Y.; Domen, K. *Nature* **2006**, *440*, 295.
(10) Maeda, K.; Teramura, K.; Lu, D.; Saito, N.; Inoue, Y.; Domen, K. *Angew. Chem., Int. Ed.* **2006**, *45*, 7806−9.

(11) Maeda, K.; Teramura, K.; Saito, N.; Inoue, Y.; Kobayashi, H.; Domen, K. *Pure Appl. Chem.* **2006**, *78*, 2267−2276.
(12) Lee, Y.; Terashima, H.; Shimodaira, Y.; Teramura, K.; Hara, M.; Kobayashi, H.; Domen, K.; Yashima, M. *J. Phys. Chem. C* **2007**, *111*, 1042−1048.
(13) Lehn, J. M.; Sauvage, J. P.; Ziessel, R. *Nouv. J. Chim.* **1979**, *3*, 423−7.
(14) Brunschwig, B. S.; Chou, M. H.; Creutz, C.; Ghosh, P.; Sutin, N. *J. Am. Chem. Soc.* **1983**, *105*, 4832−3.
(15) Ghosh, P. K.; Brunschwig, B. S.; Chou, M.; Creutz, C.; Sutin, N. *J. Am. Chem. Soc.* **1984**, *106*, 4772−83.
(16) Hurst, J. K. *Coord. Chem. Rev.* **2005**, *249*, 313−328.
(17) Baffert, C.; Romain, S.; Richardot, A.; Lepretre, J.-C.; Lefebvre, B.; Deronzier, A.; Collomb, M.-N. *J. Am. Chem. Soc.* **2005**, *127*, 13694.
(18) Zong, R.; Thummel, R. P. J. *Am. Chem. Soc.* **2005**, *127*, 12802−3.
(19) Morris, N. D.; Suzuki, M.; Mallouk, T. E. *J. Phys. Chem. A* **2004**, *108*, 9115.
(20) McEvoy, J. P.; Brudvig, G. W. *Chem. Rev.* **2006**, *106*, 4455−4483.
(21) Oki, A. R.; Morgen, R. J. *Synth. Commun.* **1995**, *25*, 4093.
(22) Donnici, C. L.; Filho, D. H. M.; Cruz, M.; Teixeira dos Reis, F.; Cordeiro, E. S.; Ferreira de Oliveira, I. M.; Carvalho, S.; Paniago, E. B. *J. Braz. Chem. Soc.* **1998**, *9*, 455−460.
(23) Montalti, M.; Wadhwa, S.; Kim, W. Y.; Kipp, R. A.; Schmehl, R. H. *Inorg. Chem.* **2000**, *39*, 76.
(24) Sullivan, B. P.; Salmon, D. J.; Meyer, T. J. *Inorg. Chem.* **1978**, *17*, 3334−3341.
(25) Nazeeruddin, M. K.; Zakeeruddin, S. M.; Humphry-Baker, R.; Jirousek, M.; Liska, P.; Valchopoulos, N.; Shklover, V.; Fischer, C.-H.; Grätzel, M. *Inorg. Chem.* **1999**, *38*, 6298−6305.
(26) Zabri, H.; Gillaizeau, I.; Bignozzi, C. A.; Caramori, S.; Charlot, M.-F.; Cano-Boquera, J.; Odobel, F. *Inorg. Chem.* **2003**, *42*, 6655−6666.
(27) Sprintschnik, G.; Sprintschnik, H.; Kirsch, P. P.; Whitten, D. G. *J. Am. Chem. Soc.* **1977**, *99*, 4947−4954.
(28) Park, H.; Bae, E.; Lee, J.-J.; Park, J.; Choi, W. *J. Phys. Chem. B* **2006**, *110*, 8740−8749.
(29) Hara, M.; Waraska, C. C.; Lean, J. T.; Lewis, B. A.; Mallouk, T. E. *J. Phys. Chem. A* **2000**, *104*, 5275.
(30) Harriman, A.; Thomas, J. M.; Millward, G. R. *New J. Chem.* **1987**, *11*, 757.
(31) Nahor, G. S.; Hapiot, P.; Neta, P.; Harriman, A. *J. Phys. Chem.* **1991**, *95*, 616.
(32) Kiwi, J.; Gratzel, M. *J. Am. Chem. Soc.* **1979**, *101*, 7214.
(33) Kiwi, J.; Gratzel, M. *Nature* **1979**, *285*, 657.
(34) Harriman, A.; Pickering, I. J.; Thomas, J. M.; Christensen, P. A. *J. Chem. Soc., Faraday Trans. 1* **1988**, *84*, 2795.
(35) Flynn, C. M.; Demas, J. N. *J. Am. Chem. Soc.* **1974**, *96*, 1960.
(36) Rasmussen, S. C.; Richter, M. M.; Yi, E.; Place, H.; Brewer, K. J. *Inorg. Chem.* **1990**, *29*, 3926.
(37) Vlcek, A. A.; Dodsworth, E. S.; Pietro, W. J.; Lever, A. P. B. *Inorg. Chem.* **1995**, *34*, 1906.
(38) Resch, U.; Fox, M. A. *J. Phys. Chem.* **1991**, *95*, 6316.
(39) Resch, U.; Fox, M. A. *J. Phys. Chem.* **1991**, *95*, 6169.
(40) When bicarbonate was excluded from the solution, similar kinetics were observed with 0.42 mM succinate−IrO_2 ($k_{obs} = 4.6 \times 10^3$ s^{-1}).
(41) Comparison of time-resolved photoluminescence data for $[Ru(dcb)_2(bpy(SA)_2)]^{6-}$−$IrO_2$ shows a ∼95% attenuation in the time-zero amplitude relative to $[Ru(dcb)_2(bpy(SA)_2)]^{6-}$ along with a weak, long-lived 375 ns component. The 28 ns process was not observed and is beyond time-resolution of our instrument.
(42) Asbury, J. B.; Anderson, N. A.; Hao, E.; Ai, X.; Lian, T. *J. Phys. Chem. B* **2003**, *107*, 7376−86.
(43) Asbury, J. B.; Wang, Y.; Lian, T. *J. Phys. Chem. B* **1999**, *103*, 6643−7.